Stable Light-Emitting Diodes Using Phase-Pure Ruddlesden–Popper Layered Perovskites

Hsinhan Tsai, Wanyi Nie, Jean-Christophe Blancon, Constantinos C. Stoumpos, Chan Myae Myae Soe, Jinkyoung Yoo, Jared Crochet, Sergei Tretiak, Jacky Even, Aditya Sadhanala, Giovanni Azzellino, Roberto Brenes, Pulickel M. Ajayan, Vladimir Bulović, Samuel D. Stranks, Richard H. Friend, Mercouri G. Kanatzidis, and Aditya D. Mohite**

State-of-the-art light-emitting diodes (LEDs) are made from high-purity alloys of III–V semiconductors, but high fabrication cost has limited their widespread use for large area solid-state lighting. Here, efficient and stable LEDs processed from solution with tunable color enabled by using phase-pure 2D Ruddlesden–Popper (RP) halide perovskites with a formula $(CH_3(CH_2)_3NH_3)_2(CH_3NH_3)_{n-1}Pb_nI_{3n+1}$ are reported. By using vertically oriented thin films that facilitate efficient charge injection and transport, efficient electroluminescence with a radiance of 35 W Sr^{-1} cm^{-2} at 744 nm with an ultralow turn-on voltage of 1 V is obtained. Finally, operational stability tests suggest that phase purity is strongly correlated to stability. Phase-pure 2D perovskites exhibit >14 h of stable operation at peak operating conditions with no droop at current densities of several Amperes cm^{-2} in comparison to mixtures of 2D/3D or 3D perovskites, which degrade within minutes.

Lighting comprises at least 30% of the total energy consumption across the world because of the low efficiency of those conventional fluorescence or incandescent bulbs in which most of the energy is lost through thermal radiation.[1–3] Solid-state lighting employs highly fluorescent semiconductors in light-emitting diodes (LEDs) in which light emission occurs from the radiative recombination of electrically injected carriers. This is considered to be the most promising avenue for reducing the fraction of national energy consumption from lighting by up to 75%.[4] State-of-the-art commercial LEDs are fabricated using high-quality, direct band-gap III–V group semiconductors such as GaAs and GaN but their use is curbed by their high cost of fabrication, thus limiting their appealing deployment at large-scale lighting applications.[5] On the other hand, tremendous progress has been made over the past two decades on using low-cost solution-processed semiconductors such as colloidal quantum dots (QDs)[6–9] and organic semiconductors.[10–12] Specifically, the emission from quantum dots can be tuned by changing their size and hence quantum confinement effects, thus making them highly promising for display technologies.[6] However, as the driving current in these LEDs is increased to high current densities, the external quantum efficiency (EQE) drops due to Auger recombination

H. Tsai, Dr. W. Nie, Dr. J.-C. Blancon, Dr. A. D. Mohite
Materials Physics and Application Division(MPA-11)
Los Alamos National Laboratory
P.O. Box 1663, Los Alamos, NM 87545, USA
E-mail: amohite@lanl.gov

Dr. J. Yoo, Dr. S. Tretiak
Center for Integrated Nanotechnologies(CINT)
Los Alamos National Laboratory
P.O. Box 1663, Los Alamos, NM 87545, USA

Dr. J. Crochet
Physical Chemistry and Applied Spectroscopy(C-PCS)
Los Alamos National Laboratory
P.O. Box 1663, Los Alamos, NM 87545, USA

H. Tsai, Prof. P. M. Ajayan
Department of Materials Science and Nanoengineering
Rice University
Houston, TX 77005, USA

Dr. C. C. Stoumpos, Dr. C. M. M. Soe, Prof. M. G. Kanatzidis
Department of Chemistry
Department of Materials Science and Engineering and
Argonne-Northwestern Solar Energy Research (ANSER) Center
Northwestern University
Evanston, IL 60208, USA
E-mail: m-kanatzidis@northwestern.edu

Prof. J. Even
Fonctions Optiques pour les Technologies de l'Information
FOTON UMR 6082
CNRS
INSA de Rennes, 35708 Rennes, France

Dr. A. Sadhanala, Dr. S. D. Stranks, Prof. R. H. Friend
Cavendish Laboratory
Department of Physics
University of Cambridge
Cambridge CB3 0HE, UK

Dr. G. Azzellino, R. Brenes, Prof. V. Bulović, Dr. S. D. Stranks
Research Laboratory of Electronics
Massachusetts Institute of Technology
Cambridge, MA 02139, USA

DOI: 10.1002/adma.201704217

(also known as "efficiency droop") and is considered an issue in III–V LEDs,[13–15] QD LEDs,[16,17] and organic LEDs (OLEDs).[18,19] This effect limits the achievable brightness in LEDs and hinders these materials for use in electrically injected lasers, which require high current densities.[20]

Recently, the emergence of bulk hybrid halide perovskites with the tunable band gap along with high photoluminescence quantum yield (PLQY), as well as low-cost deposition and efficient charge transport properties, enable proof-of-concept perovskite LEDs (PeLEDs) to be demonstrated. The first report by Friend and co-workers have shown bright, near-infrared (NIR) and green LEDs using the 3D perovskites $MAPbX_3$ (X = Br or I) as emitter with EQE up to 0.7%.[21] Building on this work, other groups have performed systematic contact engineering to improve the efficiency above 2%.[22–25] More recently, the peak EQE of PeLEDs reached 10% by confining the electrically injected carriers into nanograins[26,27] or quantum wells[28–33] with different sizes, which can efficiently funnel charge carriers to the lowest band-gap material and facilitate efficient radiative recombination. Moreover, motivated by the ease of band-gap tunability through tuning of the halides (X) in the hybrid perovskite materials, other groups have reported promising perovskite materials using $CsPbX_3$ nanocrystals by tuning the composition of the halide and the metal cation to achieve tunable color tunability with EQE approaching 6%.[23,34]

While these are encouraging results, the operational stability of PeLEDs is a major concern. The state-of-the-art 3D PeLED devices degrade within minutes or within a few voltages sweeps.[32,35] Furthermore, phase segregation of the mixed halides, which makes the color tuning possible, could seriously undermine stability and color purity for PeLEDs.[36,37]

2D $(R)_2(CH_3NH_3)_{n-1}Pb_nI_{3n+1}$ Ruddlesden–Popper layered perovskites (RPLPs) are a class of semiconducting materials[38–40] consisting of layers of defined thickness (n value) separated by organic cations (**Figure 1**a) that were shown to be promising low-cost materials with superior stability for photovoltaics[41–46] and optoelectronics.[22,28,29,31–33,47–52] Efficient PeLEDs were recently demonstrated by employing RPLPs with graded n distributions to achieve NIR LEDs with high EQE, enabled by energy transfer from the higher band gap (or lower n) to the lowest band-gap (larger n) RPLP regions in the mixed phase with emission energy close to that of bulk 3D perovskites.[29] Recent breakthrough by Stoumpos and co-workers demonstrated for the first time an innovative approach to obtain phase-pure RP perovskites with $n > 2$,[38,45,51,53] which in principle can enable color tunable LEDs by changing the quantum well thickness (or n number). Following that, our recent work[43] on using these phase-pure RP perovskite photovoltaics has shown that, by controlling the layer orientation while producing near single-crystalline thin films, excellent photovoltaic performance coupled with a record photostability for a perovskite cell under standard illumination has been achieved. These aspects combined together provide an opportunity to investigate the impact of phase purity of RP perovskites on the LED operational stability and color tunability,[54] which has not yet been addressed and is critical for potential light-emission applications.

Here, we report the first demonstration of bright LEDs using phase-pure 2D RPLPs with good operational stability, low turn-on voltage, and negligible efficiency droop at high current injection level. We obtain a high radiance value of ≈35 W Sr^{-1} cm^{-2} at 744 nm for $(BA)_2(MA)_4Pb_5I_{16}$ ($n = 5$, Pb_5) and ≈15 W Sr^{-1} cm^{-2} at 733 nm for $(BA)_2(MA)_3Pb_4I_{13}$ ($n = 4$, Pb_4), where BA is butylammonium and MA is methylammonium with a low sub-band-gap turn-on voltage of 1 and 1.3 V, respectively. We measure an average of 0.5% with a peak value of 1% using integrating sphere. Remarkably, we do not observe a decrease in efficiency for ultrahigh current injection (≈1–5 A cm^{-2}). Finally, we show that phase-pure RP-PeLEDs exhibit near peak operational stability of 14 h in contrast to the 3D $MAPbI_3$ or 2D/3D mixture-based PeLEDs, thus demonstrating that phase purity is strongly correlated with stability.

Figure 1 illustrates the phase purity and thin-film crystallinity of RPLPs. Figure 1a shows the crystal structures we use for this study, $(BA)_2(MA)_3Pb_4I_{13}$ (Pb_4, top) and $(BA)_2(MA)_4Pb_5I_{16}$ (Pb_5, bottom). In the crystal structure, n defines the thickness of the inorganic slabs, which are separated by an organic cation BA.[38,45] Figure 1b displays the high-resolution powder X-ray diffraction (PXRD)

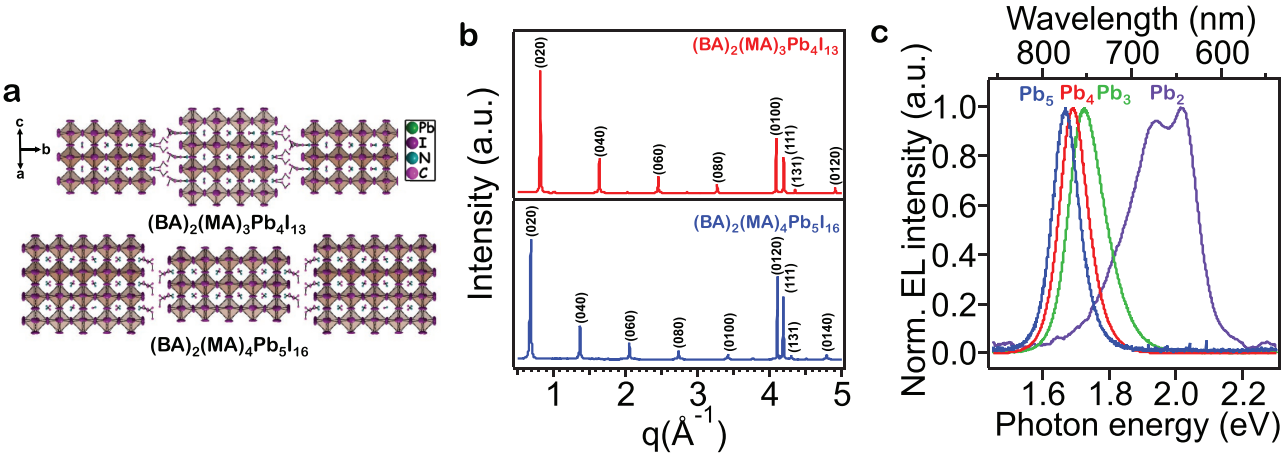

Figure 1. Structural characterization of phase-pure 2D Ruddlesden–Popper perovskites. a) The crystal structure of the top) Ruddlesden–Popper $(BA)_2(MA)_3Pb_4I_{13}$ and bottom) $(BA)_2(MA)_4Pb_5I_{16}$ layered perovskites. b) PXRD of $(BA)_2(MA)_3Pb_4I_{13}$ and $(BA)_2(MA)_4Pb_5I_{16}$ powder indicating equally spaced (0k0) peaks at low angle, which are the signature for pure phase of synthesized materials. c) Demonstration of tunable EL with well-defined n units in the pure phase Ruddlesden–Popper perovskites.

patterns for $(BA)_2(MA)_3Pb_4I_{13}$ (red curve) and $(BA)_2(MA)_4Pb_5I_{16}$ (blue curve), which shows equally spaced low-angle Bragg peaks between a q value of 0 and 4 representing (0k0) planes, where the number of (0k0) Bragg peaks corresponds to the n value of the RPLPs. The spectra for each compound only show one set of peaks, which is a clear signature of phase purity. We note here that as the n values increases it becomes increasingly more difficult to stabilize pure phases, a mixture of phases with different n values can form without carefully controlling the chemical reaction.

Having achieved phase purity of the 2D perovskites, we incorporate these into LED devices to demonstrate RP-PeLEDs as illustrated Figure 1c, which shows electroluminescence (EL) spectra of devices fabricated with n = 2, 3, 4, 5 as the emission layer. The emission peak can be tuned from NIR for Pb_5 (744 nm) down to a visible range for Pb_2 (616 nm). This is a direct consequence of growing the thin films from phase-pure RPLP single crystals (Figure S1, Supporting Information, and Figure 1b for PXRD) that eliminates impurities from other higher n numbers or 3D phases in the thin film. In films with mixtures (phase impure), the injected carriers can cascade from the higher band gap ($n \approx 1$–5) to the lower energy 3D-like states belonging to the high n values ($n > 10$) thus compromising color tunability through systematic quantum-well confinement.

Our recently developed hot-casting method[43,55–58] was applied to deposit thin films of RP perovskites. **Figure 2**a illustrates the perovskite crystal structural evolution of $(BA)_2(MA)_3Pb_4I_{13}$ for the different hot-casting temperatures measured using synchrotron grazing-incidence wide-angle X-ray scattering (GIWAXS). With progressively increasing the casting temperature from RT to 150 °C, we observe a transformation from the ring-like Debye Scherer pattern to discrete Bragg spots, which is a strong indication of a highly crystalline and oriented film. From the data, one could observe the evolution of (101) peak being more intense in the Z-direction (out-of-plane direction) as temperature increases. The orientation of the Bragg spots (110) and (202) in the reciprocal space indicates that the inorganic perovskite slabs are aligned vertically (out of plane) with respect to the substrate.[43] We further found that the substrate hydrophilicity also plays a

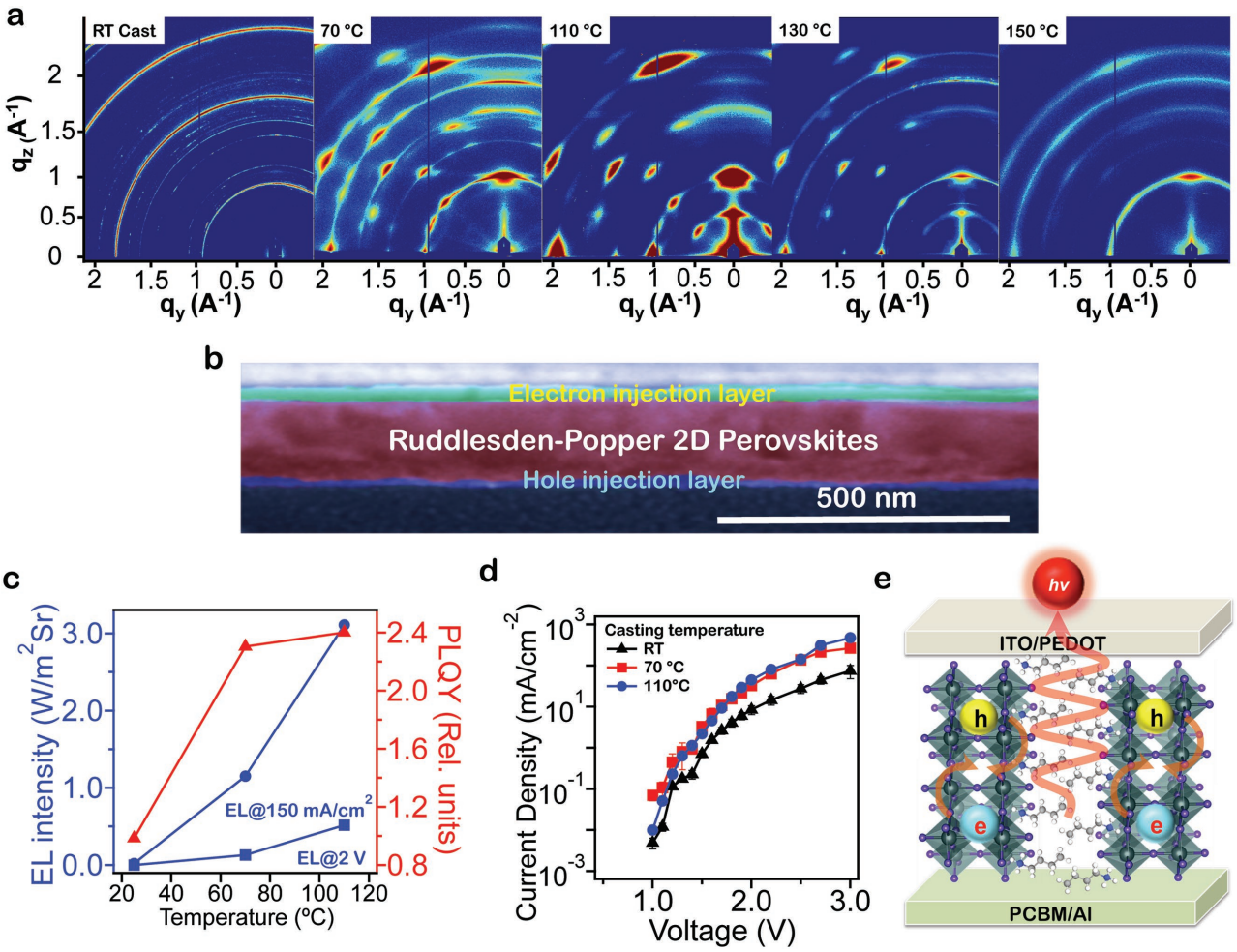

Figure 2. Thin-film morphology characterization and orientation-dependent electroluminescence from phase-pure Ruddlesden–Popper perovskites. a) GIWAXS map of $(BA)_2(MA)_3Pb_4I_{13}$ thin films with progressively increasing casting temperature (RT to 150 °C). b) Cross-sectional SEM image for the LED device configuration. c) EL intensity as a function of casting temperature at a fixed current density and fixed voltage left) and PLQY as a function of casting temperature right) for $(BA)_2(MA)_2Pb_4I_{13}$ (Pb_4) LEDs. d) J–V characteristic curve for LEDs using $(BA)_2(MA)_2Pb_4I_{13}$ casted by different temperatures. e) Scheme illustration of the charge injection/recombination process in oriented film.

role in the oriented film formation (as presented in Figure S2 with discussions in the Supporting Information).

Based on the above analysis, we tentatively propose a mechanism on thin film growth. We believe thermal energy (here temperature) is the key factor to assist crystalline thin film growth with preferential orientation. Besides, the surface energy of the substrate can also assist the polar inorganic slab of layered perovskites to grow along out-of-plane direction. We note that further increasing the casting temperature above 130 °C disrupts the strong vertical orientation and crystallinity as seen from the appearance of a ring-like pattern in the GIWAXS again. This may be due to the thermal instability of the BA or MA molecule.[59] The highly oriented thin films are homogenously deposited on the planar substrate, and are compact and pinhole free as illustrated in the cross-sectional scanning electron microscopy (SEM) image in Figure 2b.

Motivated by the vertical orientation of the perovskite slabs we fabricated bright RP-PeLEDs in the architectures and investigated the EL properties as a function of hot-casting temperatures. We employ the device structure used in photovoltaic planar device, using poly(3,4-ethylenedioxythiophene) polystyrene sulfonate (PEDOT:PSS) as a hole injection layer (HIL) and [6,6]-phenyl-C61-butyric acid methyl ester (PCBM) as an electron injection layer. Figure 2c shows the EL intensity as a function of processing temperature. Overall, the devices processed at higher temperature (70 and 110 °C) demonstrate much higher EL intensity as compared to the RT-processed device, which reflects the better vertical orientation as inferred from the GIWAXS pattern in Figure 2a. As the hot-casting temperature increases (i.e., degree of vertical alignment of the slabs improves), the device EL intensity increases rapidly when driven at the same forward voltage (dots) by ≈1500 times and by ≈150 times when driven at the same current density (square). Moreover, the hot-cast device (110 °C) has a much steeper slope in the range of ≈1–3 V in comparison to the lower temperature processed devices (RT and 70 °C), further suggesting a high recombination rate after charge injection in the device. We also examined the photoluminescence properties of those films by performing the PL spectrum and PLQY on the film (see Figure 2c and the Experimental Section, and discussion in the Supporting Information), and the PL emission peak corresponds to the band edge value with high emission efficiency compared to the 3D perovskites. The PLQY for high-temperature processed films is in the range of 2.4%, which is ≈2.5 times higher than the room temperature processed films. This increase in PLQY mainly results from the improvement of the crystallinity of the perovskite films as demonstrated by the PL full width-at-half-maximum analysis and the upper band carrier relaxation measurements carried out by excitation-energy-dependent PL intensity measurement (see also Figure S3 in the Supporting Information). These measurements suggest that the hot-cast film with superior crystallinity reduces the electronic impurity both below the gap and near the upper band, which prevents the photoexcited carrier from being scattered when excited at high energy or captured when emitting through the band edge. Both the improvements lead to 2.5 times increase in PLQY.

The charge injection and transport properties in the RP-PeLEDs were assessed by measuring the current-density–voltage characteristics (*J*–*V* curve) for different hot-casting temperatures and are illustrated in Figure 2d. The hot-cast devices (110 and 70 °C) exhibit a high current density in comparison to the RT cast devices for the same applied voltage, indicating efficient charge injection from the contact into the 2D perovskites. The results imply that crystalline and oriented films are not affected by deep level trap states, and majority of the photogenerated carriers recombine radiatively through the band gap.

From the EL device study, we found the efficient charge injection and transport facilitate radiative recombination in the vertically aligned thin films (110 °C), which systematically reduces for the 70 °C and RT-processed thin films. We attribute the high injection current for the 110 °C device to the near single-crystalline nature of the vertically aligned inorganic slabs with respect to the substrate that can form conductive channels across the two injecting electrodes as proposed in the scheme in Figure 2e. Moreover, when comparing the EL intensities while driving at the same current density, the hot-cast device exhibits 1500 times higher radiance values (Figure 2c). This indicates that radiative recombination efficiency is much higher in the oriented films at the same injection current level. The increase is beyond the PLQY increase for oriented film (2.5 times higher); we could thus conclude that by orienting the conducting inorganic channels electrons and holes are allowed to be injected and transported deeper into the center of the thin films, and thus increasing the probability of radiative recombination rather than carrier loss via nonradiative processes close to the contact interfaces.

We further optimized the device contact layers (see contact engineering results in Table S1 in the Supporting Information) to achieve bright PeLEDs using Pb_4 and Pb_5 as emission layers and evaluated the LED performance including the turn-on voltage, radiance-current–voltage curve and external quantum efficiency as summarized in **Figure 3**. As illustrated in Figure 3a, the turn-on voltages use Pb_4 or Pb_5 as emission layer across 10 devices. The average value of the turn-on voltage is 1.0 and 1.3 V for Pb_4 and Pb_5, respectively, which is far below the optical band gap of these materials (1.68 and 1.66 eV; see EL and PL spectra in Figure S4 in the Supporting Information). This represents a record for the lowest turn-on voltage value reported for any PeLEDs.[60] The turn-on voltage is similar to the open-circuit voltage of the solar cell, which represents the quasi-Fermi level splitting in the device. We believe that this benefits from the efficient injection of the carriers from the contact to the inorganic perovskite layers, without potential loss by crossing the energy barriers (potentially from BA organic cation). The device radiance and current density as a function of applied forward bias are shown in Figure 3b. From the curves, we observe a linear increase in log-radiance–voltage curve in both $n = 4$ and $n = 5$ cases. In the same operating regime, we also observe linear increase for the *J*–*V* characteristics. The slope of the *J*–*V* curve in the 1–2 V regime is an indication of the nature of charge recombination in the device. The fact that the emission increases monotonically with injection current, is indicative of an efficient radiative recombination in the device by the injected charges in both Pb_4 and Pb_5 devices. Furthermore, the PL and EL spectra for Pb_4 and Pb_5 lie on top of one another (Figure S4 in the Supporting Information), which suggests that the radiative recombination in the device originates from recombination in the emission layer. The above results suggest that the phase-pure crystalline thin films used in RP-PeLEDs can be driven at

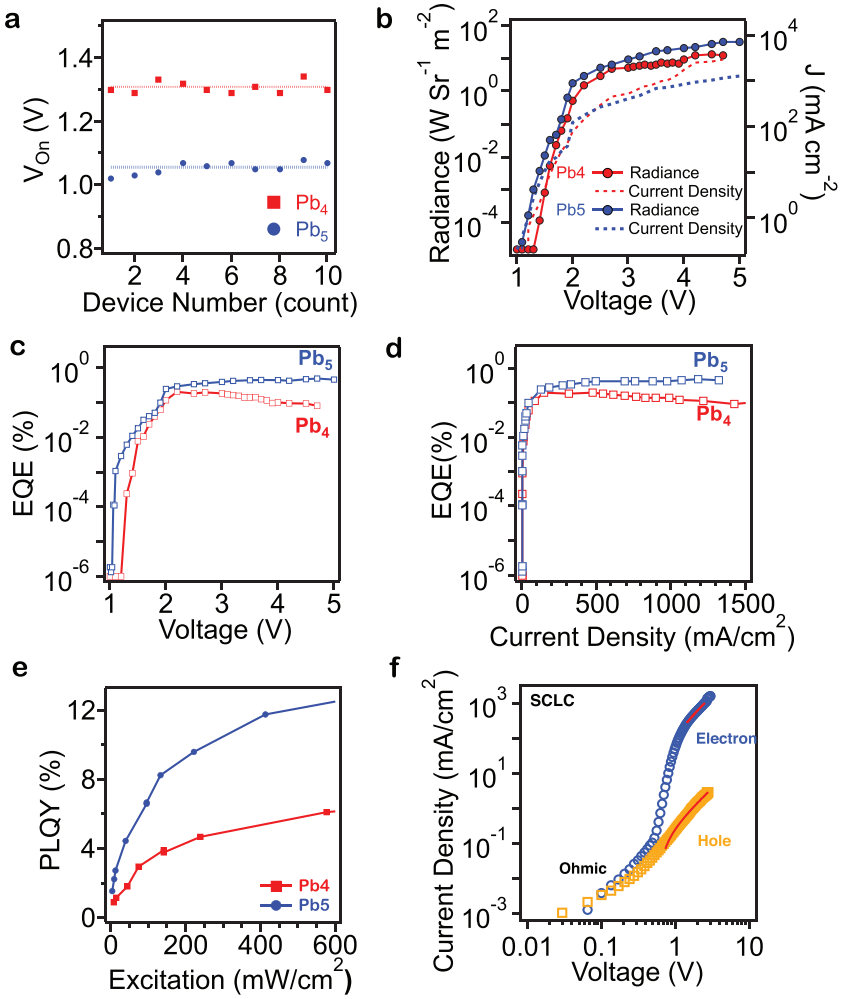

Figure 3. Measurements of photoemission and figure of merit for RP-PeLEDs. a) Turn-on voltage of the electroluminescence in PeLED devices over ten devices. b) Radiance and current-density–voltage curves for Pb_4 and Pb_5 devices in optimized structure. EQE curve as a function of c) forward voltage and d) injected current density for Pb_4 and Pb_5 RPL-PeLEDs in the optimized device configuration. e) PLQY of both Pb_4 and Pb_5 materials in the region of excited carriers relevant to LED operation. f) SCLC measurement for electron–hole mobility of Pb_5 devices.

very low operating voltage with high radiance in comparison to an applied 5–10 V reported on mixed phase 2D and 3D perovskite-based LEDs.[22,33,60]

We calculate the EQE of the optimized device using Pb_4 and Pb_5 as emission layer as illustrated in Figure 3c,d. The planar LED emission follows Lambertian profile as illustrated in Figure S5 in the Supporting Information. We measured the EQE using both a calibrated silicon detector (see the Experimental Section for details) and an integrating sphere to capture the light emitted from the front surface. From the results, we found that EQE values reach a maximum of 0.2% and 0.5% for Pb_4 and Pb_5 devices, respectively (see Figure 3c,d), and both methods are consistent with obtained EQE values (see Figure S6 in the Supporting Information). The EQE reaches its peak value after low driving voltage of 2 V and saturates for higher applied voltage. The relatively higher EQE for Pb_5 compared to Pb_4 is consistent with the higher PLQY results in Figure 3e. In addition, we also find that the PLQY of these films reach values of 12% (see discussion in the Supporting Information), two orders of magnitude higher than the 3D counterpart,[29,61,62] demonstrating their potential for light emission devices.

Although our EQE value for the RP-PeLED device is much higher than the 3D counterpart (≈0.01% shown in Figure S7 in the Supporting Information) in the same device configuration, the absolute value (≈1%) is still lower than that has been reported in the literature with other organic cations.[29,30,33] To understand the origin of lower measured EQE, we further evaluated our thin-film properties with PLQY under excitation power similar to the electrical injection level. From our PLQY data (Figure 3e and discussion in the Supporting Information), the external emission efficiency in neat films is 8.5% at an excitation density that is equivalent to the injection current at 2 V. Considering the PLQY as the radiative recombination upper limit at this charge density for this material, the EL device is emitting 12% of the total radiative recombination (excitation source was a continuous wave(CW) 561 nm laser).

In addition, we performed space charge limited current (SCLC) measurements[63] in order to understand charge carrier mobility in the RPLP planar devices. We measured the current-density–voltage curves for hole-only and electron-only devices for hot-cast Pb_5 devices (see the Experimental Section for device structure) and the results are shown in Figure 3f. We can fit the curve by the Mott–Gurney space charge model[64,65] for both the devices at a voltage range of 1–5 V, while below 1 V the current follows the Ohms law as expected. The result demonstrates that the electron-only device has 2 orders higher current than the hole-only device in the space charge limited region ($J \sim V^2$), which manifests a much higher mobility for electron in the RPLP device than the hole mobility. Such electron and hole mobility imbalance could originate from the carrier localization near the interface of inorganic/organic cation in the molecule, which is intrinsic to the materials.[38] However, the imbalanced electron and hole mobility in the high injection region could lead to the flow of a large current at high voltage level, passing through the device without any significant radiative recombination at the center of the film, leading to low quantum efficiency in the LED at high voltage.

In summary, the intrinsic PLQY (no outcoupling) is moderate ranging from 5% to 10% at excitation densities similar to the injection current density and thus undermines the emission efficiency in the phase-pure 2D RPLPs with butylamine as the organic cation. Moreover, by examining of the device properties by SCLC measurement, we observed a higher electron mobility than the hole mobility at the high current injection region. These experiments reveal the origin of lower EQE

value during device operation. Improvements are expected through charge carrier confinement in vertical direction, manipulation of film morphology, or contact engineering for achieving balanced charge injection and transport. The possible mechanism causes low EQE and detailed discussion can be found in Section S9 in the Supporting Information. In addition, further improvement in EQE is expected by modifying the organic molecules to achieve high PLQY and balanced electron and hole mobility through carrier confinement, chemical engineering of electronic edge states as suggested by the reports[26,27,50] through film morphology manipulation.

Next, we highlight two novel aspects of the RP-PeLEDs fabricated by using phase-pure 2D RLLPs and highly crystalline thin films with vertically oriented slabs. First, for Pb_5-based LEDs, after reaching a peak EQE at 2.5 V, both the radiance and EQE values tend to saturate without showing degradation. We emphasize that even for enormous injection current densities (1329 mA cm^{-2} at 5 V), the EQE value for Pb_5 device does not roll off while that for Pb_4 device it only exhibits a very small droop (Figure 3d). Droop may occur at even higher current density, which however tends to damage the electrodes.

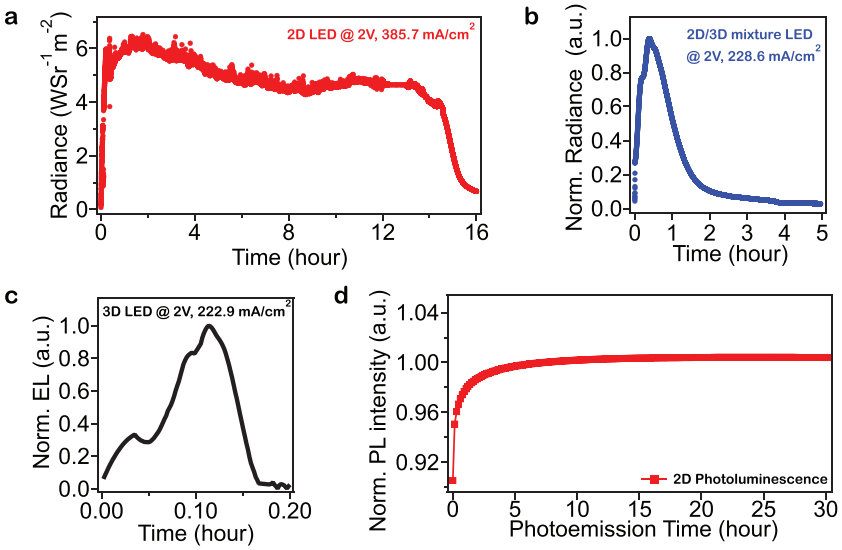

Figure 4. Stability tests on RP-PeLEDs under operation condition. LED device lifetime measurements of a) 2D, b) quasi-2D (or 2D/3D) mixture and c) 3D PeLEDs under fix operation bias (2 V) by monitoring the EL intensity change as a function of operating time in hour. d) PL stability measurement for 2D perovskites with 690 nm laser and 220 mw cm^{-2} illumination under vacuum.

In contrast, the efficiency droop with conventional GaAs, QDLED, and OLED devices generally occurs at similar carrier densities (≈10^2–10^3 mA cm^{-2}) as we drive our RP-PeLEDs. The Auger recombination process is one of the possible explanations proposed to explain the efficiency droop.[13,15,17–19] We may expect that fundamental Auger processes to be different in perovskite materials by comparison to III–V classical semiconductors.[66,67] In fact, recent optical measurements on $MAPbI_3$ using four-wave mixing techniques reveal weaker many-body interactions than the reference GaAs sample used in that study as alternative explanations for the efficiency droop,[68] such as unbalanced electron and hole carrier injection cannot be ruled out and will be explored in future studies. Nevertheless, our results suggest that higher order processes associated with efficiency droop do not dominate in the present measurement here for the 2D RP-PeLEDs, even for large current densities of a few A cm^{-2}. The operation of the RP perovskite structures at very high current densities demonstrates their promise as candidates for electrically injected lasing applications.

Finally, for a successful technology based on RP-PeLEDs and future exploration of RP perovskite based lasers, scrutinizing the device lifetime under optimal operating conditions is critical. Operation lifetime or stability of perovskite-based LEDs has been rarely reported.[35] Here, we present a comprehensive report on the stability as a function of time of Pure phase RP-PeLEDs encapsulated with a glass cover slip by monitoring the peak radiance value over time while driving constantly at forward bias with a large current injection. **Figure 4** shows the time evolution of RP-PeLED radiation using highly oriented, Pb_4 thin film (hot cast at 110 °C) as an emission layer driven at a voltage of 2 V and a high current density of 385.7 mA cm^{-2} (Figure 4a) emitting at a radiance value of 6 W Sr^{-1} m^{-2}. For comparison, we performed the same stability testing for devices fabricated with a 2D/3D mixture by mixing 20% 3D perovskites in the Pb_4 precursor (Figure 4b) and pure 3D perovskites (Figure 4c) as emission layers using the same device structure and testing conditions, and the EL intensities were normalized for those devices. The RP-PeLEDs fabricated using phase-pure Pb_4 show good stability over 14 h under continuous operation with negligible loss in its radiance. In contrast, PeLEDs fabricated with 2D/3D mixtures as shown in Figure 4b, degrades within 1 h of continuous operation when driven at the same applied voltage (2 V, 223.9 mA cm^{-2}) and the pure 3D PeLEDs degrade in less than 10 min operating under similar condition (2 V, 222.9 mA cm^{-2}) in Figure 4c. The results indicate that the 3D-like components in the 2D perovskite thin films can be detrimental to the device lifetime under constant operating current. This means growing the RP perovskite thin film from Pure phase 2D perovskite compound is key step toward achieving stable device operation in PeLEDs.

After 14 h of continuous operation, the RP-PeLEDs also experience a drop in radiance. We believe that this arises from the corrosion (or degradation) of the contacts (perovskite/aluminum or PEDOT: PSS) and not from the intrinsic degradation of the 2D RPLP emission layer. To test our hypothesis, we monitored the PL intensity (690 nm laser with 220 mW cm^{-2} power) of an isolated film of 2D perovskite prepared using identical conditions to those used for device fabrication with a photoexcited charge density that is comparable to the injected current flow through the PeLEDs as illustrated in Figure 4d. We did not observe any degradation in PL intensity implying that the observed degradation in radiance likely results from corrosion at the interfaces or contacts. Furthermore, the corrosion of

the contacts is also clearly visible in the device. These results suggest that phase-pure 2D RPLP films offer excellent intrinsic stability and are ideal for low-energy consuming RP-PeLEDs and other optoelectronic applications.

In summary, we demonstrate a stable, bright light-emitting diode based on a 2D Ruddlesden–Popper layered perovskites with phase purity. Our study suggests fabrication route toward stable and efficient light-emitting diodes with color tunability achieved by tuning the quantum well thickness. These RP-PeLEDs can be operated at low turn-on voltages of 1 V and driven at high current density of few A cm^{-2} without observable degradation. Finally, we demonstrate that use of phase-pure 2D layered perovskite offers a viable and superior solution for stable LED device operation.

Experimental Section

Materials and Instruments: PEDOT:PSS (3–4 wt% in H_2O), lead oxide, butylammine (BA, 99%), methylamine hydrochloride (MACl), phenyl-C61-butyric acid methyl ester (PCBM, >99.5%), *N,N′*-bis(3-methylphenyl)-*N,N′*-diphenylbenzidine (TPD, 99%), bathocuproine (BCP, 99.99%), 2,2′,2″-(1,3,5-benzinetriyl)-tris(1-phenyl-1-*H*-benzimidazole) (TPBi, >99.5%), hydriodic acid (HI, 57 wt% in H_2O), hypophosphorous acid (H_3PO_2, 50% in H_2O), and *N,N*-dimethylformamide (DMF, anhydrous) were purchased from Sigma-Aldrich. All the materials were used as received without further purification. EL spectra were obtained by Ocean Optics USB-4000. Brightness is calculated from measuring the photocurrent of the calibrated Si diode (thorlabs, FDS100-Cal) with known spectrum response.

Materials Synthesis: The synthesis of the layered 2D perovskite, $(BA)_2(MA)_{n-1}Pb_nI_{3n+1}$, has been reported elsewhere.[38,45,51] Generally, layered 2D perovskite materials were prepared by combining PbO, MACl, and BA in appropriate ratios in an HI/H_3PO_2 solvent mixture as described previously. For high resolution powder X-ray diffraction, we exposed the bulk RPLP crystals directly with synchrotron source.

Device Fabrication: The RP perovskite precursor solutions were prepared with 0.225 M of Pb^{2+} concentration and stirred at room temperature for overnight followed by previous report.[43,50,51] Layered 2D perovskite light-emitting diodes were prepared with the structure of ITO/hole transporting layer (HTL)/2D RP perovskite/electron transporting layer (ETL)/Al (Figure 2b). The emitting layers were fabricated using our previously developed hot-casting method[43,55–58] with layered 2D perovskite crystals in DMF. The HTL and ETL contacts are prepared by spin casting (PEDOT:PSS and PCBM) or thermal evaporating (TPD, BCP, and TPBi) followed by thermal deposition with top electrode (aluminum metal, 100 nm) in a vacuum chamber, and shadow mask area of 0.035 cm^2 was used to define the working area.

After preparing the devices, the UV-curable epoxy was dropped over the electrodes with a small cover glass placed on top to seal the devices. The perovskite thin films for optical measurements are prepared on a glass substrate using the same method as described above. The SCLS measurements used device architecture ITO/TiO_2/2D RP perovskite/PCBM/Al for the electron-only device and ITO/PEDOT:PSS/2D perovskite/PTAA/Al for the hole-only device.

Device Characterization: All RP-PeLED devices characterizations were carried out with encapsulation at room temperature. The electroluminescence spectra and brightness of RP-PeLEDs were collected by ocean optics spectrometer at the same integration time. The radiance–voltage curves are collected by applying voltage with Keithley 2400 unit and collecting radiance value by the calibrated silicon diode (FDS100-Cal, Thor Labs) with known spectral response. The Si diode was kept at a distance with the testing device and the solid angle can thus be calculated from the area of the cell, distance, and the area of the diode. The lifetime data were recorded constantly with the silicon diode.

Absolute absorption and PLQY of the thin films were measured with integrating sphere, following previous report,[69] in air under ambient conditions. Measurements were obtained directly after taking the samples out of vacuum to minimize effects of air exposure which were found to be negligible for about 1 h,[43] and some of the samples were encapsulated for cross-checking the data. Alternatively, we performed these measurements in an in-lab-build microscope, in which case the samples are under vacuum (10^{-5} to 10^{-6} Torr) and verify a meaningful set of data points using the integrating sphere. For PL measurements, we used a CW laser emitting at 561 nm for excitation and spectral responses were recorded through a spectrograph (Spectra-Pro 2300i) and a CCD camera (EMCCD 1024B) yielding a maximum error of 2 nm. The absorption spectra were measured using a broadband white light lamp.

The angular dependence of the EL was obtained by fixing the orientation of an LED and measuring the EL spectra for different angles with respect to the normal to the LED front surface (the EL was collected with a 400 μm fiber placed at a constant distance of about 50 cm from the LEDs).

SCLC measurements used the electron- or hole-only devices with scan range from −1.0 to +5 .0 V and the curves were fitted by the Mott–Gurney space charge model.[64,65] Synchrotron GIWAXS measurements were performed at Beamline sector 8-ID-E of the Advanced Photon Source at Argonne National Laboratory. All the RPLP samples prepared on Si-wafer/PEDOT:PSS substrates were exposed to an X-ray beam (λ = 1.6868 Å) with an incident angle of 0.15° and exposed for 5 s, and the scattered light was collected by a Pilatus 1 M pixel array detector at 204 mm from the sample. GIWAXS data were processed using the GIXSGUI package[70] for Matlab (Mathworks) with correction for detector sensitivity, X-ray polarization, and geometrical solid angle.

Supporting Information

Supporting Information is available from the Wiley Online Library or from the author.

Acknowledgements

H.T. and W.N. contributed equally to this work. The work at LANL was supported by LANL LDRD program (A.D.M., W.N., G.G., J.-C.B., and S.T.) and Institute for Materials Science (IMS) Rapid Response (H.T). The work at Northwestern University was supported ONR (N00014-17-1-2231) is acknowledged (MGK). The authors would like to acknowledge the technical support provided by Dr. Joseph W. Strzalka for synchrotron measurements with fruitful discussions, and the use of the Advanced Photon Source at Argonne National Laboratory was supported by the US Department of Energy, Office of Science, Office of Basic Energy Sciences, under Contract No. DE-AC02-06CH11357. The research leading to these results at Massachusetts Institute of Technology has received funding from the People Programme (Marie Curie Actions) of the European Union's Seventh Framework Programme (FP7/2007-2013) under REA grant agreement number PIOF-GA-2013-622630.

Conflict of Interest

The authors declare no conflict of interest.

Keywords

color tunability, crystal orientation, LEDs, Ruddlesden–Popper layered perovskites

Received: July 27, 2017
Revised: October 10, 2017
Published online: January 3, 2018

[1] I. Ahemen, K. D. Dilip, A. N. Amah, *Appl. Phys. Res.* **2014**, *6*, 95.
[2] E. F. Schubert, J. K. Kim, *Science* **2005**, *308*, 1274.
[3] B. W. D'Andrade, S. R. Forrest, *Adv. Mater.* **2004**, *16*, 1585.
[4] Department of Energy, http://energy.gov/eere/ssl/about-solid-state-lighting-program. (Accessed date: November 2016)
[5] J. H. Burroughes, D. D. C. Bradley, A. R. Brown, R. N. Marks, K. Mackay, R. H. Friend, P. L. Burns, A. B. Holmes, *Nature* **1990**, *347*, 539.
[6] Y. Shirasaki, G. J. Supran, M. G. Bawendi, V. Bulovic, *Nat Photonics* **2013**, *7*, 13.
[7] L. Sun, J. J. Choi, D. Stachnik, A. C. Bartnik, B.-R. Hyun, G. G. Malliaras, T. Hanrath, F. W. Wise, *Nat. Nanotechnol.* **2012**, *7*, 369.
[8] J. M. Caruge, J. E. Halpert, V. Wood, V. Bulovic, M. G. Bawendi, *Nat. Photonics*, **2008**, *2*, 247.
[9] B. S. Mashford, M. Stevenson, Z. Popovic, C. Hamilton, Z. Zhou, C. Breen, J. Steckel, V. Bulovic, M. Bawendi, S. Coe-Sullivan, P. T. Kazlas, *Nat. Photonics*, **2013**, *7*, 407.
[10] S. Reineke, F. Lindner, G. Schwartz, N. Seidler, K. Walzer, B. Lussem, K. Leo, *Nature* **2009**, *459*, 234.
[11] P. K. H. Ho, J.-S. Kim, J. H. Burroughes, H. Becker, S. F. Y. Li, T. M. Brown, F. Cacialli, R. H. Friend, *Nature* **2000**, *404*, 481.
[12] M. A. Baldo, D. F. O'Brien, Y. You, A. Shoustikov, S. Sibley, M. E. Thompson, S. R. Forrest, *Nature* **1998**, *395*, 151.
[13] J. Iveland, L. Martinelli, J. Peretti, J. S. Speck, C. Weisbuch, *Phys. Rev. Lett.* **2013**, *110*, 177406.
[14] S. Pimputkar, J. S. Speck, S. P. DenBaars, S. Nakamura, *Nat. Photonics*, **2009**, *3*, 180.
[15] M.-H. Kim, M. F. Schubert, Q. Dai, J. K. Kim, E. F. Schubert, J. Piprek, Y. Park, *Appl. Phys. Lett.* **2007**, *91*, 183507.
[16] X. Gong, Z. Yang, G. Walters, R. Comin, Z. Ning, E. Beauregard, V. Adinolfi, O. Voznyy, E. H. Sargent, *Nat. Photonics*, **2016**, *10*, 253.
[17] W. K. Bae, Y.-S. Park, J. Lim, D. Lee, L. A. Padilha, H. McDaniel, I. Robel, C. Lee, J. M. Pietryga, V. I. Klimov, *Nat. Commun.* **2013**, *4*, 2661.
[18] J. Kalinowski, W. Stampor, J. Mężyk, M. Cocchi, D. Virgili, V. Fattori, P. Di Marco, *Phys. Rev. B* **2002**, *66*, 235321.
[19] Y. Shirasaki, G. J. Supran, W. A. Tisdale, V. Bulović, *Phys. Rev. Lett.* **2013**, *110*, 217403.
[20] L. A. Coldren, S. W. Corzine, M. L. Mašanović, in *Diode Lasers and Photonic Integrated Circuits*, (Ed: Kai Chang) John Wiley & Sons, Inc., Hoboken, New Jersey, **2012**, p. 157.
[21] Z.-K. Tan, R. S. Moghaddam, M. L. Lai, P. Docampo, R. Higler, F. Deschler, M. Price, A. Sadhanala, L. M. Pazos, D. Credgington, F. Hanusch, T. Bein, H. J. Snaith, R. H. Friend, *Nat. Nanotechnol.* **2014**, *9*, 687.
[22] A. Vassilakopoulou, D. Papadatos, I. Zakouras, I. Koutselas, *J Alloys Compd.* **2017**, *692*, 589.
[23] X. Zhang, B. Xu, J. Zhang, Y. Gao, Y. Zheng, K. Wang, X. W. Sun, *Adv. Funct. Mater.* **2016**, *26*, 4595.
[24] J. Wang, N. Wang, Y. Jin, J. Si, Z.-K. Tan, H. Du, L. Cheng, X. Dai, S. Bai, H. He, Z. Ye, M. L. Lai, R. H. Friend, W. Huang, *Adv. Mater.* **2015**, *27*, 2311.
[25] Y.-H. Kim, H. Cho, J. H. Heo, T.-S. Kim, N. Myoung, C.-L. Lee, S. H. Im, T.-W. Lee, *Adv. Mater.* **2015**, *27*, 1248.
[26] Z. Xiao, R. A. Kerner, L. Zhao, N. L. Tran, K. M. Lee, T.-W. Koh, G. D. Scholes, B. P. Rand, *Nat. Photonics*, **2017**, *11*, 108.
[27] H. Cho, S.-H. Jeong, M.-H. Park, Y.-H. Kim, C. Wolf, C.-L. Lee, J. H. Heo, A. Sadhanala, N. Myoung, S. Yoo, S. H. Im, R. H. Friend, T.-W. Lee, *Science* **2015**, *350*, 1222.
[28] D. N. Congreve, M. C. Weidman, M. Seitz, W. Paritmongkol, N. S. Dahod, W. A. Tisdale, *ACS Photonics* **2017**, *4*, 476.
[29] M. Yuan, L. N. Quan, R. Comin, G. Walters, R. Sabatini, O. Voznyy, S. Hoogland, Y. Zhao, E. M. Beauregard, P. Kanjanaboos, Z. Lu, D. H. Kim, E. H. Sargent, *Nat. Nanotechnol.* **2016**, *11*, 872.
[30] N. Wang, L. Cheng, R. Ge, S. Zhang, Y. Miao, W. Zou, C. Yi, Y. Sun, Y. Cao, R. Yang, Y. Wei, Q. Guo, Y. Ke, M. Yu, Y. Jin, Y. Liu, Q. Ding, D. Di, L. Yang, G. Xing, H. Tian, C. Jin, F. Gao, R. H. Friend, J. Wang, W. Huang, *Nat. Photonics*, **2016**, *10*, 699.
[31] D. Liang, Y. Peng, Y. Fu, M. J. Shearer, J. Zhang, J. Zhai, Y. Zhang, R. J. Hamers, T. L. Andrew, S. Jin, *ACS Nano* **2016**, *10*, 6897.
[32] H. Hu, T. Salim, B. Chen, Y. M. Lam, *Sci. Rep.* **2016**, *6*, 33546.
[33] J. Byun, H. Cho, C. Wolf, M. Jang, A. Sadhanala, R. H. Friend, H. Yang, T.-W. Lee, *Adv. Mater.* **2016**, *28*, 7515.
[34] Y.-H. Kim, H. Cho, T.-W. Lee, *Proc. Natl. Acad. Sci. USA* **2016**, *113*, 11694.
[35] N. Wang, L. Cheng, R. Ge, S. Zhang, Y. Miao, W. Zou, C. Yi, Y. Sun, Y. Cao, R. Yang, Y. Wei, Q. Guo, Y. Ke, M. Yu, Y. Jin, Y. Liu, Q. Ding, D. Di, L. Yang, G. Xing, H. Tian, C. Jin, F. Gao, R. H. Friend, J. Wang, W. Huang, *Nat. Photonics*, **2016**, *10*, 699.
[36] D. J. Slotcavage, H. I. Karunadasa, M. D. McGehee, *ACS Energy Lett.* **2016**, *1*, 1199.
[37] E. T. Hoke, D. J. Slotcavage, E. R. Dohner, A. R. Bowring, H. I. Karunadasa, M. D. McGehee, *Chem. Sci.* **2015**, *6*, 613.
[38] C. C. Stoumpos, D. H. Cao, D. J. Clark, J. Young, J. M. Rondinelli, J. I. Jang, J. T. Hupp, M. G. Kanatzidis, *Chem. Mater.* **2016**, *28*, 2852.
[39] L. Pedesseau, D. Sapori, B. Traore, R. Robles, H.-H. Fang, M. A. Loi, H. Tsai, W. Nie, J.-C. Blancon, A. Neukirch, S. Tretiak, A. D. Mohite, C. Katan, J. Even, M. Kepenekian, *ACS Nano* **2016**, *10*, 9776.
[40] C. R. Kagan, D. B. Mitzi, C. D. Dimitrakopoulos, *Science* **1999**, *286*, 945.
[41] X. Zhang, X. Ren, B. Liu, R. Munir, X. Zhu, D. Yang, J. Li, Y. Liu, D.-M. Smilgies, R. Li, Z. Yang, T. Niu, X. Wang, A. Amassian, K. Zhao, S. Liu, *Energy Environ. Sci.* **2017**.
[42] K. Yao, X. Wang, Y.-x. Xu, F. Li, L. Zhou, *Chem. Mater.* **2016**, *28*, 3131.
[43] H. Tsai, W. Nie, J.-C. Blancon, C. C. Stoumpos, R. Asadpour, B. Harutyunyan, A. J. Neukirch, R. Verduzco, J. J. Crochet, S. Tretiak, L. Pedesseau, J. Even, M. A. Alam, G. Gupta, J. Lou, P. M. Ajayan, M. J. Bedzyk, M. G. Kanatzidis, A. D. Mohite, *Nature* **2016**, *536*, 312.
[44] L. Mao, H. Tsai, W. Nie, L. Ma, J. Im, C. C. Stoumpos, C. D. Malliakas, F. Hao, M. R. Wasielewski, A. D. Mohite, M. G. Kanatzidis, *Chem. Mater.* **2016**, *28*, 7781.
[45] D. H. Cao, C. C. Stoumpos, O. K. Farha, J. T. Hupp, M. G. Kanatzidis, *J. Am. Chem. Soc.* **2015**, *137*, 7843.
[46] I. C. Smith, E. T. Hoke, D. Solis-Ibarra, M. D. McGehee, H. I. Karunadasa, *Angew. Chem., Int. Ed.* **2014**, *53*, 11232.
[47] L. Cheng, Y. Cao, R. Ge, Y.-Q. Wei, N.-N. Wang, J.-P. Wang, W. Huang, *Chin. Chem. Lett.* **2017**, *28*, 29.
[48] M. Wei, W. Sun, Y. Liu, Z. Liu, L. Xiao, Z. Bian, Z. Chen, *Phys. Status Solidi A* **2016**, *213*, 2727.
[49] A. Vassilakopoulou, D. Papadatos, I. Koutselas, *Appl. Mater. Today* **2016**, *5*, 128.
[50] J.-C. Blancon, H. Tsai, W. Nie, C. C. Stoumpos, L. Pedesseau, C. Katan, M. Kepenekian, C. M. M. Soe, K. Appavoo, M. Y. Sfeir, S. Tretiak, P. M. Ajayan, M. G. Kanatzidis, J. Even, J. J. Crochet, A. D. Mohite, *Science*, **2017**, 355, 1288.
[51] C. C. Stoumpos, C. M. M. Soe, H. Tsai, W. Nie, J.-C. Blancon, D. H. Cao, F. Liu, B. Traoré, C. Katan, J. Even, A. D. Mohite, M. G. Kanatzidis, *Chem* **2017**, *2*, 427.
[52] B. Liu, C. M. M. Soe, C. C. Stoumpos, W. Nie, H. Tsai, K. Lim, A. D. Mohite, M. G. Kanatzidis, T. J. Marks, K. D. Singer, *Solar RRL* **2017**, *1*, 1700062.
[53] C. M. M. Soe, W. Nie, C. C. Stoumpos, H. Tsai, J.-C. Blancon, F. Liu, J. Even, T. J. Marks, A. D. Mohite, M. G. Kanatzidis, *Adv. Energy. Mater.*, https://doi.org/10.1002/aenm.201700979.
[54] G. Li, F. W. R. Rivarola, N. J. L. K. Davis, S. Bai, T. C. Jellicoe, F. de la Peña, S. Hou, C. Ducati, F. Gao, R. H. Friend, N. C. Greenham, Z.-K. Tan, *Adv. Mater.* **2016**, *28*, 3528.

[55] W. Nie, H. Tsai, R. Asadpour, J.-C. Blancon, A. J. Neukirch, G. Gupta, J. J. Crochet, M. Chhowalla, S. Tretiak, M. A. Alam, H.-L. Wang, A. D. Mohite, *Science* **2015**, *347*, 522.
[56] H. Tsai, W. Nie, P. Cheruku, N. H. Mack, P. Xu, G. Gupta, A. D. Mohite, H.-L. Wang, *Chem. Mater.* **2015**, *27*, 5570.
[57] W. Nie, J.-C. Blancon, A. J. Neukirch, K. Appavoo, H. Tsai, M. Chhowalla, M. A. Alam, M. Y. Sfeir, C. Katan, J. Even, S. Tretiak, J. J. Crochet, G. Gupta, A. D. Mohite, *Nat. Commun.* **2016**, *7*, 11574.
[58] H. Tsai, W. Nie, Y.-H. Lin, J. C. Blancon, S. Tretiak, J. Even, G. Gupta, P. M. Ajayan, A. D. Mohite, *Adv. Energy Mater.* **2017**, *7*, 1602159.
[59] S. J. Kulkarni, C. V. Kavedia, *Thermochim. Acta* **1994**, *246*, 71.
[60] S. A. Veldhuis, P. P. Boix, N. Yantara, M. Li, T. C. Sum, N. Mathews, S. G. Mhaisalkar, *Adv. Mater.* **2016**, *28*, 6804.
[61] J. M. Richter, M. Abdi-Jalebi, A. Sadhanala, M. Tabachnyk, J. P. H. Rivett, L. M. Pazos-Outón, K. C. Gödel, M. Price, F. Deschler, R. H. Friend, *Nat. Commun.* **2016**, *7*, 13941.
[62] S. D. Stranks, V. M. Burlakov, T. Leijtens, J. M. Ball, A. Goriely, H. J. Snaith, *Phys. Rev. Appl.* **2014**, *2*, 034007.
[63] C. Goh, R. J. Kline, M. D. McGehee, E. N. Kadnikova, J. M. J. Fréchet, *Appl. Phys. Lett.* **2005**, *86*, 122110.
[64] S. A. Moiz, I. A. Khan, W. A. Younis, K. S. Karimov, in *Conducting Polymers* (Ed: F. Yilmaz), InTech, Rijeka **2016**, Ch. 5.
[65] M. Kiy, P. Losio, I. Biaggio, M. Koehler, A. Tapponnier, P. Günter, *Appl. Phys. Lett.* **2002**, *80*, 1198.
[66] J. Even, L. Pedesseau, C. Katan, M. Kepenekian, J.-S. Lauret, D. Sapori, E. Deleporte, *J. Phys. Chem. C* **2015**, *119*, 10161.
[67] A. Haug, *J. Phys. C: Solid State Phys.* **1983**, *16*, 4159.
[68] S. A. March, C. Clegg, D. B. Riley, D. Webber, I. G. Hill, K. C. Hall, *Sci. Rep.* **2016**, *6*, 39139.
[69] J. C. de Mello, H. F. Wittmann, R. H. Friend, *Adv. Mater.* **1997**, *9*, 230.
[70] Z. Jiang, X. Li, J. Strzalka, M. Sprung, T. Sun, A. R. Sandy, S. Narayanan, D. R. Lee, J. Wang, *J. Synchrotron Radiat.* **2012**, *19*, 627.